Available online at www.sciencedirect.com
ScienceDirect
Journal of Power Sources 179 (2008) 286–291
JOURNAL OF POWER SOURCES
www.elsevier.com/locate/jpowsour

Short communication

Performance evaluation of several commercial alloys in a reducing environment

Y. Liu *

Department of Mechanical Engineering, Box 5014, Tennessee Technological University, 115W, 10th Street, Cookeville, TN 38505, USA

Received 4 November 2007; received in revised form 19 December 2007; accepted 19 December 2007
Available online 27 December 2007

Abstract

Several commercial alloys including Ebrite, Crofer 22 APU, Haynes 230 and Haynes 242, which are candidates for intermediate-temperature solid oxide fuel cell (SOFC) interconnect materials, were isothermally and cyclically oxidized at 900 °C in the reducing atmosphere of Ar + 5 vol.% H_2 + 3 vol.% H_2O corresponding to the SOFC anode environment. Results indicate that these alloys exhibited good scale spallation resistance with the Ni-base alloys possessing better oxidation resistance over the Fe-base alloys. Both Mn–Cr spinel and Cr_2O_3 were formed in the oxide scales of these alloys. For Crofer 22 APU and Haynes 242, a continuous protective MnO and Mn–Cr spinel layer formed outside on the inner layer of Cr_2O_3. The increase in scale ASR after longer-term thermal exposure in the reducing environment was relatively slower for the Ni-base alloys than for the Fe-base alloys.

Keywords: Alloys; SOFC; Interconnect; Cyclic oxidation; Reducing atmosphere

1. Introduction

Solid oxide fuel cell (SOFC) is a solid-state power generation system that directly converts the chemical energy of fossil fuels into electricity without combustion and mechanical processes. It has been extensively studied in the past decades as a promising power generation technology with high efficiency, low emission level and flexibility of fuel choices. Many of the technical challenges in the development of SOFC are materials related [1–3]. Recent progresses in SOFC development has led to the reduction in its operating temperature from about 1000 °C to the range of 600–800 °C [4–5], which widens the materials choice for stack components such as the interconnect. Metallic interconnects attract a great deal of attention due to its low cost, high electronic conductivity, high thermal conductivity, good manufacturability, and improved mechanical strength, etc., compared to traditional ceramic interconnects [6–9]. The metallic interconnects of current interest are the Cr_2O_3-forming alloys such as Ebrite, Crofer 22 APU, Haynes 230 and Haynes 242 due to the electrically conductive nature of Cr_2O_3 compared to other protective scales such as Al_2O_3 and SiO_2 [10–14].

The interconnect in a SOFC stack is exposed simultaneously to both an oxidizing atmosphere (air) on the cathode side and a reducing atmosphere (fuel, such as hydrogen) on the anode side. The stability requirement includes minimizing reactions with the electrode materials and the atmospheres while maintaining good electrical conductivity. Numerous work has been conducted for the investigation of behaviors of metallic interconnect materials exposed to the oxidizing environment [15–17], and some initial effort was also carried out to study the interconnect behaviors in dual atmospheres [18]. However, the understanding of the oxidation behaviors of the interconnect alloys in anode environment is still lacking, especially for the electrical properties of the thermally grown oxide scales on these alloys because of the technical difficulty to measure in the reducing atmosphere. The purpose of this paper is to study the oxidation behaviors of two Fe-based alloys, i.e. Ebrite and Crofer 22 APU, and two Ni-based alloys, i.e. Haynes 230 and Haynes 242 in the reducing atmosphere. Furthermore, a modified 2-probe 4-point method for electrical property measurement of the oxide scale in the reducing atmosphere was proposed and reported in this paper. The suitability of these alloys as intermediate-temperature SOFC interconnects was also discussed.

* Now at University of Connecticut, Storrs, USA. Tel.: +1 860 486 8960; fax: +1 860 486 4745.
E-mail address: yong.liu@uconn.edu.

0378-7753/$ – see front matter © 2007 Elsevier B.V. All rights reserved.
doi:10.1016/j.jpowsour.2007.12.067

Table 1
Alloy compositions (wt.%)

	Ni	Fe	Cr	Mo	W	Mn	Co	Si	Al	Cu	Ti	C	S	B	La
Ebrite		Balance	26	1		0.02		0.025				0.001	0.02		
Crofer		Balance	22			0.45		0.1	0.12		0.08	0.005	0.002		0.06
Haynes 230	Balance	3[a]	22	2	14	0.5	5[a]	0.4	0.3			0.1		0.015[a]	0.02
Haynes 242	Balance	2[a]	8	25		0.8[a]	2.5[a]	0.8[a]	0.5[a]	0.5[a]		0.03[a]		0.006[a]	

[a] Maximum.

2. Experimental

The materials used in our investigation are Ebrite, Crofer 22 APU, Haynes 230 and Haynes 242, the chemical compositions of these alloys are listed in Table 1. Rectangular samples (about 12 mm × 11 mm × 1 mm) were cut from the alloy sheets by electric discharge machining (EDM). Each sample was drilled a hole with a diameter of 1 mm on the upper center and then polished to 800 grits using SiC sand paper, ultrasonically cleaned in acetone and dried immediately before the oxidation test. A Cahn thermobalance was employed to investigate the initial oxidation kinetics of these alloys by recording the mass gain as a function of time. The samples were oxidized at 900 °C (900 °C was selected in order to expedite the oxidation process) for 100 h in the reducing atmosphere of Ar + 4 vol.% H_2 + 3 vol.% H_2O with a flowing rate of 45 ml min^{-1}. Longer-term cyclic oxidation test was also conducted to evaluate the oxidation performance and scale spallation resistance. Each cycle consisted of isothermal holding at 900 °C in the reducing atmosphere for 20 h and followed by quenching to room temperature, with a total of 50 cycles. The cumulative oxidation time for cyclic oxidation test was, therefore, 1000 h. The phase structures of the oxide scales thermally grown on the alloys were identified with X-ray diffraction (XRD). The surface morphologies and cross-sections of the oxidized samples were observed using scanning electron microscopy (SEM) with an energy-dispersive X-ray analysis attachment (EDX).

Electrical resistance of the oxidized samples was measured using a modified 2-probe 4-point method in the reducing atmosphere from 500 °C to 800 °C with a step size of 50 °C. Fig. 1 shows the schematic of the experimental setup for electrical resistance measurement. The upper and lower oxide surfaces were covered with Au paste and Au meshes with four Au leads for current supply and voltage drop measurement. Pt paste, which was widely used for corresponding measurement in the oxidizing atmosphere, was found not suitable for the reducing atmosphere because the paste was observed to penetrate into the metal substrate during the test at high temperature in the reducing environment. In our work, Au paste here was chosen in place of Pt paste for the measurement in the reducing environment to prevent such a problem. It is critical that Au paste was fired separately with the Au mesh in order to decrease or eliminate the strain in it during the firing and cooling process. The variation of voltage across the samples under different currents ranging from 1 mA to 10 mA was verified to obey the Ohm's law exactly, which indicated that the interfacial polarization was negligible within the applied current range. A constant current of 10 mA was used in all the measurement. A widely accepted parameter for scaling the electrical resistance of the oxide scales, area specific resistance (ASR), was reported here. ASR reflected both the electrical conductivity and the thickness of the oxide scale. At each temperature, the resistance (R) was calculated according to the Ohm's law, $R = V/I$. The ASR was then equal to R multiplied by the area that the Au paste covered.

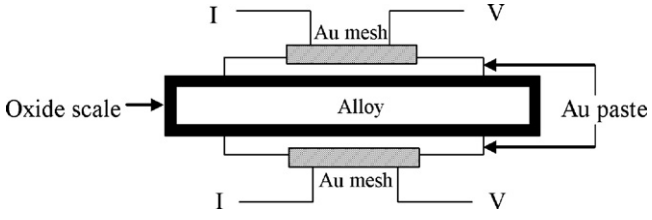

Fig. 1. Schematic of the ASR measurement setup.

3. Results and discussion

3.1. Surface morphologies and structure of the oxide scales

The XRD results of the alloys oxidized in the reducing atmosphere at 900 °C for 1000 h are given in Fig. 2, while the surface morphologies and element line scanning results of the cross-sections of these alloys are shown in Figs. 3 and 4, respectively. For the oxide scale thermally grown on Ebrite, peaks from Cr_2O_3 and $MnCr_2O_4$ were detected, as shown in Fig. 2. According to the element line scanning results, Mn element was mostly concentrated on the top surface of the oxide scale. Combining

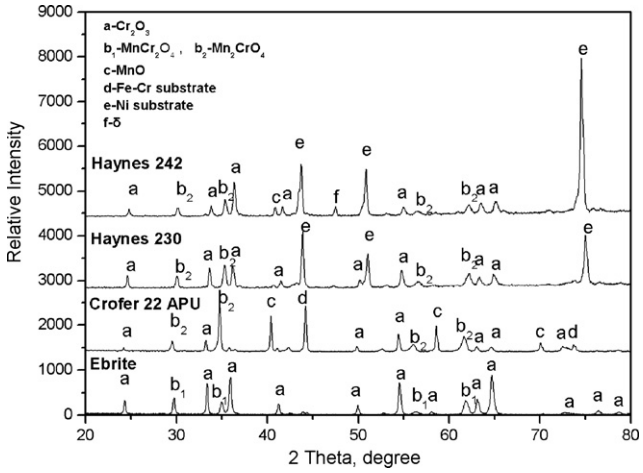

Fig. 2. XRD results of the alloys cyclically oxidized in the reducing atmosphere at 900 °C.

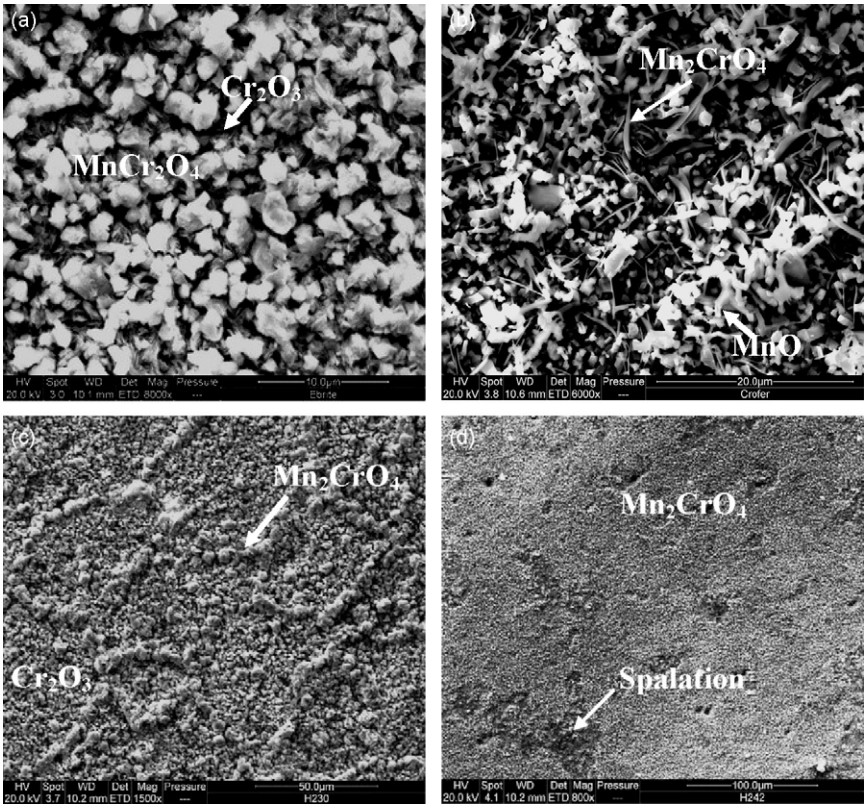

Fig. 3. Surface morphologies of the alloys: (a) Ebrite; (b) Crofer 22 APU; (c) Haynes 230; (d) Haynes 242.

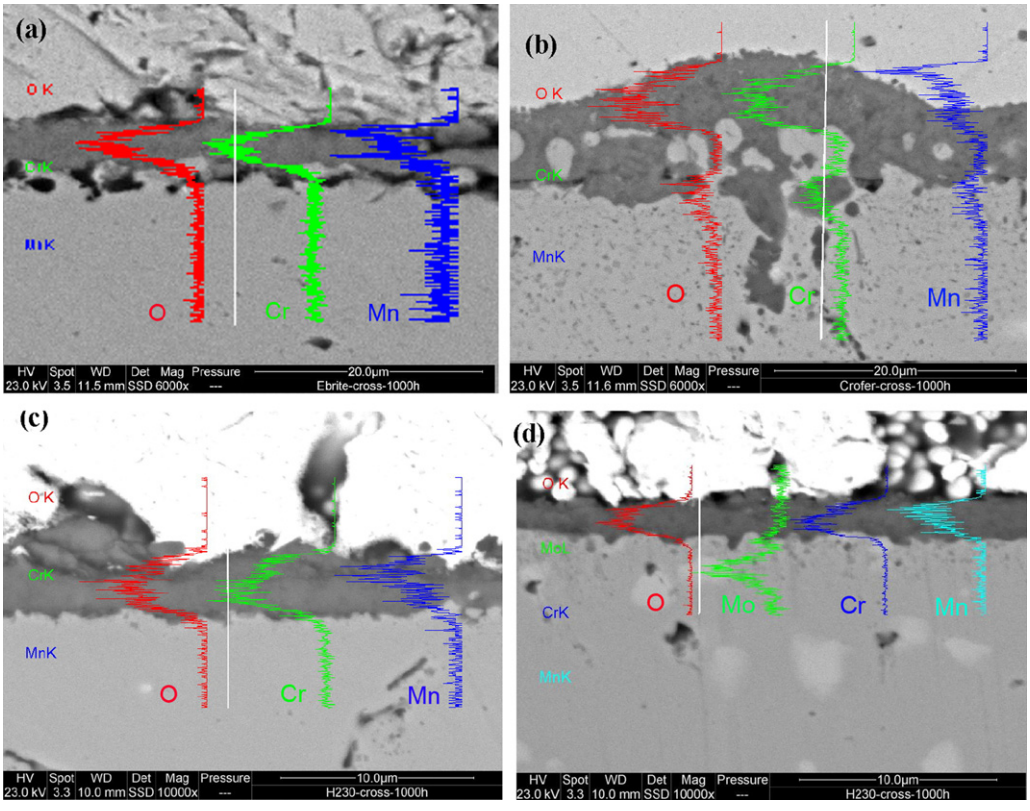

Fig. 4. Cross-sections and element line scanning results for the oxidized alloys: (a) Ebrite; (b) Crofer 22 APU; (c) Haynes 230; (d) Haynes 242.

these results with EDX analysis of the surface oxide products, the white particles on the oxide scale surface were identified as $MnCr_2O_4$, whereas the grey oxide product between the white particles was identified as Cr_2O_3. For the oxide scale on Crofer 22 APU, peaks from Cr_2O_3, Mn_2CrO_4 and MnO were detected with XRD. According to the element line scanning results, Mn was mainly distributed on the top surface of the oxide scale. Combining these results with EDX analysis of the oxide scale surface, the white oxide product on the top surface was identified as MnO, the whisker-like oxide product was identified as Mn_2CrO_4, and the Cr_2O_3 layer was beneath them as an inner layer. Based on similar analysis, the ridge-shaped oxide product on the surface of the oxide scale on Haynes 230 was Mn_2CrO_4, while the oxide between the ridges was identified as Cr_2O_3. As for the oxide scale formed on Haynes 242, a thin Mn_2CrO_4 film with small amount of MnO was formed on the top surface of the oxide scale with some features observed corresponding to the possible localized scale spallation. The Cr_2O_3 layer was under the Mn_2CrO_4 spinel film. It is noteworthy that δ phase rich in Ni and Mo elements was precipitated in the substrate after thermal exposure in the reducing environment for this alloy.

Compared to the oxide structure formed in the oxidizing environment [17], a single Cr_2O_3 layer without any Mn–Cr spinel was formed on alloy Ebrite in the oxidizing atmosphere. In the case of Crofer 22 APU in the oxidizing atmosphere, the top layer was Mn–Cr spinel, below which is the Cr_2O_3 layer, but without any MnO detected within the oxide scales. The above difference for Ebrite and Crofer 22 APU in various atmospheres might indicate that the Mn element in the reducing atmosphere more favorably diffuses out of the oxide layer to form its oxides with or without other element in contrast with that in the oxidizing environment: even though the content of Mn in Ebrite is significantly lower than other alloys, sufficient amount of Mn element diffused out of the Cr_2O_3 layer to form $MnCr_2O_4$ spinel phase. On the surface of Crofer 22 APU a sufficient amount of Mn diffused out of the Cr_2O_3 layer to react with Cr and oxygen in the environment to form the spinel phase and still a large amount of MnO. The compositions of oxide scales of Haynes 230 are similar either in the reducing or in the oxidizing environment and are mainly composed of Cr_2O_3 with small amount of Mn–Cr spinel. The morphology of oxide surface is different for that the Mn_2CrO_4 spinel formed in the reducing atmosphere is ridge-shaped. The oxide scales formed on Haynes 242 in oxidizing environment was composed of an uneven NiO outer layer and an inner Cr_2O_3 layer with Mn–Cr spinel, whereas no NiO was observed on the oxide scales in reducing environment. Since the Cr content is as low as 8 wt.%, external Cr_2O_3 layer cannot form in oxidizing environment. Then the NiO layer formed at the beginning stage. After the NiO layer was established, the oxygen partial pressure at the NiO/alloy interface decreased and the preferential oxidation of Cr occurred and led to the formation of Cr_2O_3 inner layer with small amount of Mn–Cr spinel after oxidizing environment exposure. The oxygen partial pressure in the reducing atmosphere is so low that NiO cannot be formed and Cr_2O_3 layer formed at the first stage, further oxidation is via outward diffusion of elements of Cr, Mn, etc.

3.2. Oxidation kinetics and resistance

Fig. 5 shows the mass gain and square mass gain of these alloys as a function of time. The mass gain due to oxidation increased with increasing time. According to the parabolic law $(\Delta W/A)^2 = K_p t$, where $\Delta W/A$ is the mass gain per unit area at the oxidation time, t, while K_p is the parabolic rate constant equal to the slope of the line shown in Fig. 5(b), The oxidation kinetics of Crofer 22 APU and Haynes 242 obeyed the parabolic law, whereas Haynes 230 and Ebrite deviated from the parabolic law.

Cyclic oxidation kinetics of four alloys is shown in Fig. 6. Mass gain of these alloys due to oxidation increased with increasing time, with no obvious scale spallation noticed for all the four alloys. The Ni-base alloys Haynes 230 and Haynes 242 exhibited better oxidation resistance than the Fe-base alloys Ebrite and Crofer 22 APU. The mass gain of Haynes 242 was the lowest, while that of Crofer 22 APU was the highest. As shown in Figs. 4 and 7, the oxide scale thickness was consistent with the mass gain and oxidation resistance, i.e. the thicker the oxide scale, the larger the mass gain and the less oxidation resistant for the alloy.

The isothermal oxidation kinetics of Crofer 22 APU and Haynes 242 obeyed the parabolic law. Due to the very low oxygen pressure in the reducing atmosphere, the Cr_2O_3 layer was

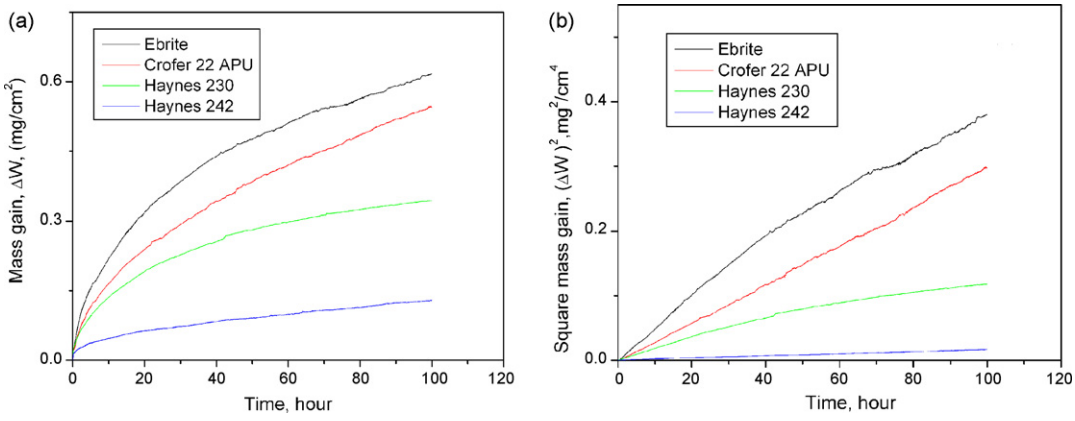

Fig. 5. Isothermal oxidation kinetics (a) and parabolic plot of the oxidation kinetics (b) of the alloys oxidized in the reducing atmosphere at 900 °C.

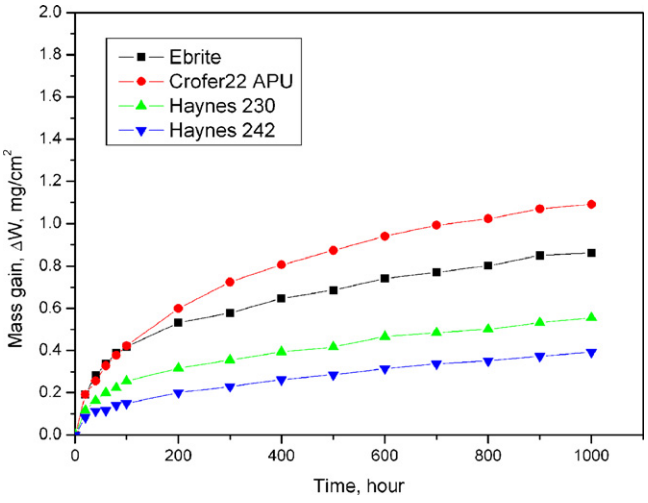

Fig. 6. Mass gain of the four alloys during cyclic oxidation in the reducing atmosphere at 900 °C.

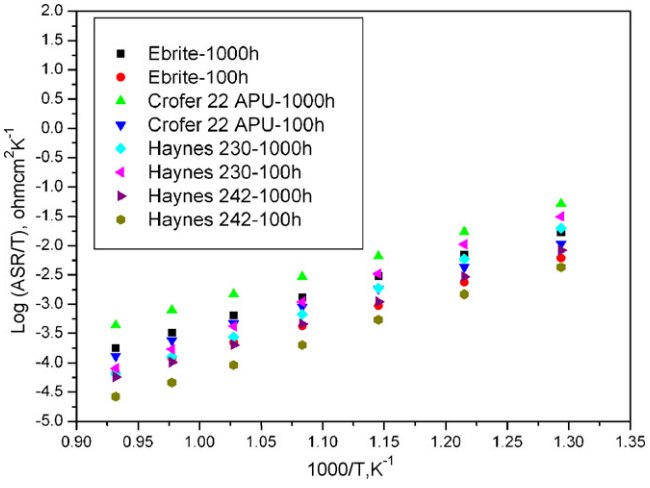

Fig. 8. Scale ASR for the alloys oxidized in reducing atmosphere at 900 °C for 100 h and 1000 h.

selectively formed initially and functioned as a blocking barrier to reduce the attack of the inner alloys. After the Cr_2O_3 was formed, further oxidation is via the outward diffusion of Cr together with other fast-diffusing elements such as Mn element through the Cr_2O_3 scale. The high diffusivity of Mn ions in Cr_2O_3 layer in the reducing environment may play an important role for the oxidation process [19]. Crofer 22 APU contains relatively high amount of Mn among these four alloys, a large amount of MnO was formed on the surface of this alloy in addition to the formation of Mn–Cr spinel, and consequently lead to the biggest mass gain. Fast diffusion of Cr and Mn caused the mass gain of Haynes 242 doubled compared to that in oxidizing environment with other similar experiment situations [20]. Significant amount of Mn diffused out of the Cr_2O_3 layer on Haynes 242 to form almost continuous Mn–Cr spinel layer and small amount of MnO, which provide protective layers to prevent the inner Cr_2O_3 from evaporation and make the oxidation obey the parabolic law.

The oxidation kinetics of Haynes 230 and Ebrite deviated from the parabolic law, possibly due to the more severe evaporation of Cr species. Mn–Cr spinel phase was not continuous enough to totally cover the Cr_2O_3 layer for these two alloys, as shown in Fig. 3. The Cr evaporation from Cr_2O_3 is expected to be substantial and much higher, consequently making the kinetics of these two alloys deviate from the parabolic law. As for Crofer 22 APU and Haynes 242, the Cr_2O_3 layer is underneath and covered by the spinel or MnO layer, thus Cr evaporation can be reduced.

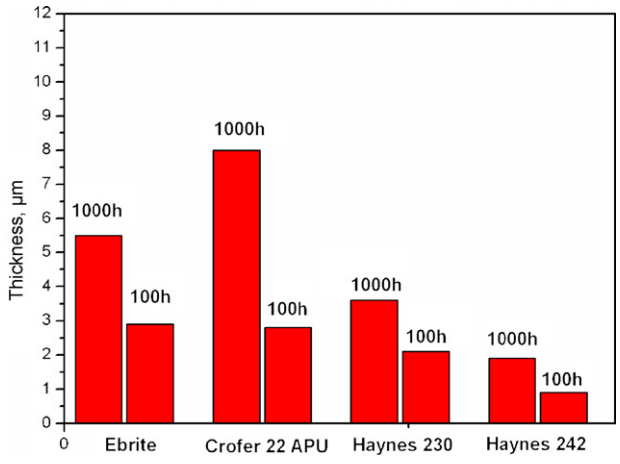

Fig. 7. Oxide scale thickness of four alloys with various exposure duration in reducing atmosphere.

3.3. Electrical resistance of the oxide scales

Fig. 8 summarized the scale ASR values for four alloys after 1000-h cyclic oxidation and 100-h isothermal oxidation. The order of the scale ASR of these alloys is consistent with the order of the oxidation resistance and the oxide scale thickness. The activation energy (E_a) for Ebrite, Crofer 22 APU and Haynes 242, calculated from the slopes in the plot [21,22], are similar, i.e. about 0.56 eV, while that of Haynes 230 is about 0.67 eV. The comparison between the ASR values of the oxide scales thermally grown after 1000 h and 100 h indicates that the scale ASR increased with the scale thickness for these four alloys except Haynes 230, but the measured E_a remained essentially unchanged. The scale ASR increased Faster with increasing scale thickness for the Fe-base alloys than for the Ni-base alloys, which is also consistent with their oxidation resistance.

The ASR value of the oxide scale is determined by the conductivity and the thickness of the oxide scale. Since Cr_2O_3 and Mn–Cr spinel are main constitutes in the oxide scales formed on Ebrite, Haynes 230 and Haynes 242 and the conductivity of spinel phase is much higher than the Cr_2O_3, the thickness of the Cr_2O_3 was a dominant factor that determines the scale ASR values of these alloys. The Ni-base alloys Haynes 230 and Haynes 242 are more oxidation resistant and form much thinner layer of Cr_2O_3 and oxide scale, as shown in Figs. 4 and 7, thus have lower ASR value than Fe-base alloys after same exposure in the reducing atmosphere. After longer-term thermal exposure in the reducing environment, the increase of the oxide scale thickness of the Ni-base alloys is expected to be slower than that of the

Fe-base alloys, which resulted in a relatively slower increase in scale ASR. That Crofer 22 APU displayed the highest ASR value resulted from a much thicker oxide scale and the possible negative role of MnO layer to increase the ASR value either due to its poor conductivity or high contact resistance with Au paste. The abnormal ASR-thickness dependence for Haynes 230 may be attributed to different oxide structures formed on the alloy's surface after exposure of different durations.

It is noteworthy that the scale electrical conductivity formed on Crofer 22 APU was higher than that on Ebrite in the oxidizing environment [17], whereas in the reducing environment the opposite results were obtained. This might be attributed to the formation of Mn–Cr spinel phase on Ebrite and MnO phase on Crofer 22 APU in the reducing atmosphere: Mn–Cr spinel phase has inherent high conductivity but MnO layer decreased oxide scale conductivity as discussed above. The scale ASR of Haynes 242 in reducing environment is significantly higher than that in the oxidizing atmosphere [17]. It might be attributed to different oxide structure formed on the alloy in different atmospheres. The oxide scale formed in air consists of a NiO top layer, Cr_2O_3 inner layer and Mn–Cr spinel, whereas in reducing environment consists of Mn_2CrO_4 spinel top layer and Cr_2O_3 inner layer with a small amount of MnO. First, The conductivity of NiO layer formed in air is about two magnitude higher than that of Cr_2O_3 at high temperature [9]; second, Cr_2O_3 processes higher conductivity in air than in reducing atmosphere with a low oxygen partial pressure [17]; third, another possible reason is that the contact resistance between the Pt and NiO is lower than that between the Au and the Mn–Cr spinel layer.

3.4. Several concerns of these alloys as SOFC interconnect

Based on this study, several concerns for these alloys to be used as SOFC interconnect can be identified. For Ebrite and Haynes 230, the Cr_2O_3 layer was not covered by a continuous protective layer and thus the Cr species evaporation or migration in long-term operation is expected to be severe and degrade the cell performance by poisoning the cathode. Porosities formed at the interface between the oxide scale and the alloy substrate for Ebrite, as shown in Fig. 4(a), might provide initiation sites for spallation in much longer-term cyclic oxidation process. As for Crofer 22 APU, the entrapment of substrate materials into the oxide scale makes the thickness of oxide scale non-uniform, as indicated in Fig. 4(b). Haynes 242 lacked thermal stability in that a Mo–Ni rich δ phase was precipitated after thermal exposure, which might be deleterious to decrease the mechanical property and oxidation resistance of the alloy. Though the Ni-base alloys process better oxidation resistance and lower oxide scale ASR values, further effort need to be carried out to reduce their relatively high CTE values corresponding to CTEs of other cell components.

4. Conclusions

Oxidation tests in the reducing environment indicate that Ebrite, Crofer 22 APU, Haynes 230 and Haynes 242 exhibited good scale spallation resistance with the Ni-base alloys possessing better oxidation resistance over the Fe-base alloys. Both Mn–Cr spinel and Cr_2O_3 were formed in the oxide scales of these alloys. For Crofer 22 APU and Haynes 242, MnO was also detected. A continuous protective outer MnO and Mn_2CrO_4 layer was formed on the oxide scales of Crofer 22 APU and Haynes 242, which is expected to reduce the evaporation of Cr species. The increase in scale ASR after longer-term thermal exposure in the reducing environment was relatively slower for the Ni-base alloys than for the Fe-base alloys.

Acknowledgements

This research was supported by the Center for Manufacturing Research, Tennessee Technological University. Special thanks are given to Oak Ridge National Lab (ORNL) for facility access and technical support.

References

[1] N.Q. Minh, J. Am. Ceram. Soc. 76 (1993) 563–588.
[2] W.A. Meulenberg, S. Uhlenbruck, E. Wessel, H.P. Buchkremer, J. Mater. Sci. 38 (2003) 507–513.
[3] J.W. Fergus, Mater. Sci. Eng. A 397 (2005) 271–283.
[4] Z. Yang, P. Singh, J.W. Stevenson, G. Xia, J. Electrochem. Soc. 153 (2006) A1873–A1879.
[5] Z. Yang, G. Xia, P.S. Singh, J.W. Stevenson, Solid State Ionics 176 (2005) 1495–1503.
[6] J.H. Zhu, Y. Zhang, A. Basu, Z.G. Lu, M. Paranthaman, D.F. Lee, E.A. Payzant, Surf. Coat. Technol. 177–178 (2004) 65–72.
[7] H. Kurokawa, K. Kawamura, T. Maruyama, Solid State Ionics 168 (2004) 13–21.
[8] G. Cabouro, G. Caboche, S. Chevalier, P. Piccardo, J. Power Sources 156 (2006) 39–44.
[9] W.Z. Zhu, S.C. Deevi, Mater. Sci. Eng. A 348 (2003) 227–243.
[10] P. Huczkowski, N. Christiansen, V. Shemet, L. Niewolak, J. Piron-Abellan, L. Singheiser, W.J. Quadakkers, Fuel Cells 2 (2006) 93–99.
[11] Z. Yang, K.S. Weil, D.M. Paxton, J.W. Stevenson, J. Electrochem. Soc. 150 (2003) A1188–A1201.
[12] M.P. Brady, B.A. Print, Z.G. Lu, J.H. Zhu, C.E. Milliken, E.D. Kreidler, L. Miller, T.R. Armstrong, L.R. Walker, Oxid. Met. 65 (2006) 237–239.
[13] Z. Yang, G. Xia, J.W. Stevenson, J. Power Sources 160 (2006) 1104–1110.
[14] N. Sakai, T. Horita, Y.P. Xiong, K. Yamaji, H. Kishimoto, M.E. Brito, H. Yokokawa, T. Maruyama, Solid State Ionics 176 (2005) 681–686.
[15] S. Geng, J.H. Zhu, J. Power Sources 160 (2006) 1009–1016.
[16] J. Pu, J. Li, B. Hua, G. Xie, J. Power Sources 158 (2006) 354–360.
[17] S. Geng, J.H. Zhu, Z.G. Lu, Scripta Mater. 55 (2006) 239–242.
[18] Z. Yang, M.S. Walker, P. Singh, J.W. Stevenson, T. Norby, J. Electrochem. Soc. 151 (2004) 669–678.
[19] F. Abe, H. Araki, H. Yoshida, M. Okada, Oxid. Met. 27 (1987) 21–36.
[20] S. Geng, J.H. Zhu, Z.G. Lu, Solid State Ionics 177 (2006) 559–568.
[21] D. England, A. Virkar, J. Electrochem. Soc. 148 (2001) 330–341.
[22] K. Huang, P.Y. Hou, J.B. Goodenough, Solid State Ionics 129 (2000) 237–250.